PCCP

PAPER

View Article Online
View Journal | View Issue

Cite this: *Phys. Chem. Chem. Phys.*, 2016, **18**, 14094

Efficient ambipolar transport properties in alternate stacking donor–acceptor complexes: from experiment to theory†

Yunke Qin,‡[ab] Changli Cheng,‡[c] Hua Geng,*[a] Chao Wang,[ab] Wenping Hu,[a] Wei Xu,*[a] Zhigang Shuai*[c] and Daoben Zhu*[a]

Received 4th March 2016,
Accepted 22nd April 2016

DOI: 10.1039/c6cp01509c

www.rsc.org/pccp

Comprehensive investigations of crystal structures, electrical transport properties and theoretical simulations have been performed over a series of sulfur-bridged annulene-based donor–acceptor complexes with an alternate stacking motif. A remarkably high mobility, up to 1.57 $cm^2 V^{-1} s^{-1}$ for holes and 0.47 $cm^2 V^{-1} s^{-1}$ for electrons, was obtained using organic single crystal field-effect transistor devices, demonstrating the efficient ambipolar transport properties. These ambipolar properties arise from the fact that the electronic couplings for both holes and electrons have the same super-exchange nature along the alternate stacking direction. The magnitude of super-exchange coupling depends not only on the intermolecular stacking distance and pattern, but also the energy level alignments between the adjacent donor–acceptor moieties. The concluded transport mechanism and structure–property relationship from this research will provide an important guideline for the future design of organic semiconductors based on donor–acceptor complexes.

Introduction

Great efforts have been devoted toward the design and synthesis of organic semiconducting materials for organic field-effect transistors (OFETs), and impressive improvements in the device performance have been achieved recently.[1–8] Ambipolar OFETs, which can transport holes and electrons simultaneously, have attracted much attention because of their potential applications for more compact complementary circuits[9,10] and ambipolar light-emitting transistors.[11,12] To some extent, organic donor–acceptor (D–A) complexes have provided an alternative avenue for ambipolar materials since the first discovery of ambipolar transport behavior of (BEDT-TTF) (F2TCNQ) (BEDT-TTF = bis(ethylenedithio)tetrathiafulvalene; F2TCNQ = 2,5-difluoro-7,7,8,8-tetracyanoquinodimethane) at low temperature by T. Hasegawa *et al.* in 2004.[13] Subsequently, the family of organic D–A complexes was stressed as another prospective channel material[14] and was proved to exhibit unique optoelectronic properties.[15–19] Recently, more ambipolar devices were fabricated with D–A complexes as active materials by the judicious combination of hole-conducting (donor) and electron-conducting (acceptor) molecules.[20–23] The integration of ambipolar transport and red photoluminescence properties was also realized based on isometric distyrylbenzene and dicyanobenzene by Park *et al.*[24] In addition, *meso*-diphenyl tetrathia[22]annulene[2,1,2,1] (DPTTA) was demonstrated to be one of the most suitable candidates as a donor molecule for the construction of DA-type semiconductors owing to its electron-rich aromatic macrocyclic structure and excellent assembling ability with acceptors.[25,26] Our recent study of a DPTTA–DTTCNQ (DTTCNQ = 4,8-bis(dicyanomethylene)-4,8-dihydrobenzo[1,2-*b*:4,5-*b*′]-dithiophene) complex exhibited high ambipolar behavior with a hole mobility of 0.77 $cm^2 V^{-1} s^{-1}$ and an electron mobility of 0.24 $cm^2 V^{-1} s^{-1}$ in an ambient atmosphere.[27] Studies on organic D–A complexes will open up an entire new avenue of research for electronic and photonic devices.[28,29]

[a] *Beijing National Laboratory for Molecular Sciences, Key Laboratory of Organic Solids, Institute of Chemistry, Chinese Academy of Sciences, Beijing 100190, P. R. China. E-mail: hgeng@iccas.ac.cn, wxu@iccas.ac.cn, zhudb@iccas.ac.cn*
[b] *University of Chinese Academy of Sciences, Beijing, 100049, P. R. China*
[c] *Chemistry Department, Tsinghua University, Beijing 100084, P. R. China. E-mail: zgshuai@tsinghua.edu.cn*

† Electronic supplementary information (ESI) available: Synthesis of SNTCNQ; growth of the self-assembled microcrystal and device fabrication; UV-Vis and FT-IR spectra; crystal data, CT characteristics of the complexes; the first redox potentials of pristine acceptors; overlap patterns (view perpendicular to the DPTTA plane) and lateral interactions between donor molecules in DPTTA-based complexes; output curves, the I_{on} and I_{off} distribution of DPTTA-based complex devices; the air-stability tests by contrast of the typical transfer curve as well as the mobility distribution of DPTTA-based complex devices; schemes of DAD and ADA triads used for hole and electron super-exchange coupling calculations; band structures of DPTTA-based complexes; valence and conduction total bandwidths and related bandwidths along the D–A mixed stacking directions. CCDC 1437142–1437144. For ESI and crystallographic data in CIF or other electronic format see DOI: 10.1039/c6cp01509c

‡ Y. Qin and C. Cheng contributed equally to this work.

Although the charge-transport properties of these complexes have been investigated for years experimentally, theoretical guidance is still insufficient toward the design and understanding of the charge-transport mechanism of D–A complexes with ambipolar transport properties. Recently, remarkable ambipolar charge-transport properties were predicted and an effective electronic coupling between adjacent donor (or acceptor) molecules was manifested by a super-exchange mechanism in mixed-stack D–A complexes.[30] Meanwhile, the wide valence and conduction bands, large hole and electron electronic couplings, and small hole and electron effective masses were summarized as key parameters for predicting and filtering D–A charge-transfer (CT) complexes with excellent ambipolar charge-transport properties.[31] Moreover, molecular insights into the electronic couplings paved the way toward the rational design of high-performance transporting materials with various charge polarities.[32] However, the calculation results may sometimes contradict the experimental data.[33]

In the case of inadequate consideration, putting the donor and acceptor together casually is not advisable and unlikely getting the desired results due to the strong relationship between the crystal geometry and the electronic, optical, and charge transport properties. In the prototype case of the TTF–TCNQ complex, the high electrical conductivity was well-known.[34] However, when dibenzotetrathiafulvalene (DBTTF) was employed as a donor molecule, the obtained DBTTF–TCNQ exhibited semiconducting properties and revealed ambipolar behavior.[20] Further, when TCNQ was replaced by 2,3,5,6-tetrafluoro-TCNQ (F4TCNQ), it resulted in DBTTF–F4TCNQ with segregated stacking and electrically insulated characteristics.[35] Obviously, to achieve a D–A complex with ambipolar transport is a challenging task. Appropriate design concept and theoretical guidance are particularly necessary due to the delicate and elusive relationship between the donor and the acceptor molecule. Thus, to gain further insights into the transport mechanism would require a more detailed, systematic and in-depth collaborative investigation both experimentally and theoretically. The introduction of novel donor and/or acceptor molecules by rationally tuning the packing mode and the donor–acceptor interactions will be likely to push devices to higher levels of performance.

In this text, we report the noncovalent assembly of a typical donor molecule DPTTA with acceptors, including 2,5-difluoro-7,7,8,8-tetracyanoquinodimethane (F2TCNQ), 2,3,5,6-tetrafluoro-7,7,8,8-tetracyanoquinodimethane (F4TCNQ) and 1,2,5-thiadiazolotetracyanoquinodimethane (SNTCNQ). The three complexes have 1 : 1 stoichiometry and crystalize in alternate-stack along the *a*-axis. The DPTTA core unit consists of four thiophene groups to form a coplanar molecular backbone, which allows the extended delocalization of the π-electrons and strong self-assembling capability with acceptors. The three new D–A complexes obtained all display efficient ambipolar transport properties along the preferential growth direction. The difference in the electron affinity of acceptors allows us to tune and optimize the transport properties. Remarkably, the F2TCNQ–DPTTA complex single crystal device reveals the highest ambipolar transport behaviors among the reported D–A system to date with the hole and electron mobility reaching up to 1.57 and 0.47 $cm^2\ V^{-1}\ s^{-1}$, respectively. Moreover, we also calculated the electronic band structure and intermolecular electronic coupling and rationalized the experimental results. The influence of packing modes and D–A interactions on the transport properties was also discussed through the combination of experimental and theoretical studies.

Experimental section

DPTTA was purchased from BioDuro, A PPD Company. The product was further purified by recrystallization (in toluene and dichloromethane). F2TCNQ, F4TCNQ were obtained from Tci and used directly without further purification.

UV-vis spectra were taken on a Hitachi U-3010 spectrometer. IR spectra were recorded on a TENSOR 27 instrument (BRUKER, GERMANY). TEM and SAED measurements were carried out on a microcrystal grown on an amorphous carbon-coated TEM grid on JEOL 2010 (Japan).

The DPTTA-based complexes used for IR were obtained as shiny black microcrystals by mixing solutions of the donor and acceptor in chlorobenzene (molar ratio 1 : 1) (Method A). In a typical procedure: DPTTA solution (11.2 mg/15 ml) in chlorobenzene was added into F2TCNQ chlorobenzene solution (4.8 mg/15 ml) carefully in a 1 : 1 molar ratio. The mixture was then placed into a darkroom without disturbance for 24 hours. The donor–acceptor complex was precipitated, which was carefully filtered and then washed with a small portion of chlorobenzene prior to vacuum drying. The rapid formation of precipitates upon mixing donor and acceptor solutions is a clear indication of charge transfer.

The single crystals of the DPTTA-based complex used for X-ray analysis were obtained by H-cell (Method B). X-ray diffraction (XRD) was carried out on Empyrean (PANalytical) with a CuKa source (κ = 1.541 Å). X-ray crystallographic data were collected using a Bruker Smart-1000-CCD diffractometer, using graphite-monochromated Mo Kα radiation (λ = 0.71073 Å).

I–V characteristics of the OFETs were recorded using a Keithley 4200 SCS and a Micromanipulator 6150 probe station in a clean and shielded box at room temperature in air. The mobilities (μ) were calculated in the saturation regime by the following equation: $I_D = \mu C_i(W/2L)(V_G - V_T)^2$, where I_D is the drain current, μ is the field-effect mobility, C_i is the gate dielectric capacitance, W and L are the channel width and length, respectively, V_G is the gate voltage, V_T is the threshold voltage.

Results and discussion

Preparation of single crystals of DPTTA-based donor–acceptor complexes

Two different methods were used for preparing single crystals of DPTTA-based D–A complexes. Method A consisted of mixing a solution of DPTTA in chlorobenzene and the corresponding acceptor (molar ratio 1 : 1) in the same solvent. The obtained solution was allowed to mix slowly and black crystals with

metallic luster were collected after 24 hours (Scheme 1). For the growth of the microcrystal suitable for device fabrication, the obtained D–A crystals were re-dissolved in chlorobenzene to get their saturated solutions. Then microcrystals suitable for FET device fabrication were obtained by drop-casting of the saturated solution onto the SiO_2/Si substrates, as illustrated in Scheme 1 [details are provided in the ESI†]. The solvent evaporation rate is believed to be critical to the formation of a well-ordered structure. A slow evaporation process that takes several hours is adopted. In Method B, DPTTA and the corresponding acceptor (molar ratio 1 : 1) powders were added separately to the two arms of a H-shaped tube. Then chlorobenzene was added separately to the two arms of the H-shaped tube. The solutions were allowed to diffuse slowly and large crystals formed in weeks. Method B gave bulk crystals, which were suitable for X-ray single crystal structure characterization.

Spectral characterization

Due to the low ionization potential (IP) of one partner and the high electron affinity (EA) of the other one, charge transfer from the donor to the acceptor molecule is expected to occur in the complexes formed. The charge transfer ratio will show impacts on the molecular conformation and stacking patterns and finally affect the electrical transport properties. The UV-vis absorption spectra of DPTTA-based complexes in dilute chlorobenzene solutions are presented in Fig. S1 (ESI†). A significant shifting of maximum absorption or the formation of a CT absorption band cannot be observed in the ground state probably due to the weak charge-transfer interaction in the solution with relatively low concentration. Whereas obvious charge transfer was clearly indicated between the donor and the acceptor in the corresponding complexes by infrared absorption spectra (IR) (Fig. S2 in the ESI†). The C≡N stretching frequency of the TCNQ derivative is known to be sensitive to the ionicity and shifts to a lower frequency region with an increase of the ionicity.[36,37] Neutral F2TCNQ, F4TCNQ and SNTCNQ show C≡N stretching bands at 2229 cm^{-1}, 2226 cm^{-1} and 2226 cm^{-1}, which shift to 2196 cm^{-1} (Δ = 33 cm^{-1}), 2191 cm^{-1} (Δ = 35 cm^{-1}) and 2219 cm^{-1} (Δ = 7 cm^{-1}) in the corresponding complexes. The large low-frequency shift suggests the highly ionized state of F2TCNQ and F4TCNQ molecules in complexes. The C≡N stretching mode shows a slight low-frequency shift in the SNTCNQ–DPTTA complex, suggesting the weakly ionized state.

Structural characterization

The evaluation of the single crystal structure is critical for understanding the electrical transport behavior observed in the single crystal FETs. The DPTTA-based complexes all crystallized in the triclinic unit cell belonging to the $P\bar{1}$ space group. The crystallographic data are collected in Table S1 (ESI†) and Fig. 1. The asymmetric unit for each complex contains one half of the donor and acceptor, as the molecules possess symmetrical centers located at the center of annulene and quinoid rings, respectively. It should be noted that in F2TCNQ–DPTTA the fluorine atom appeared in 2,3,5,6-positions of the quinoid ring with 50% occupancy (Fig. 1a). The thiadiazolo-unit in SNTCNQ–DPTTA also disordered with a site-occupancy factor of 0.5 (Fig. 1e). In the complexes, with the acceptor getting stronger, more significant distortion from the planar conformation of the sulfur bridged annulene ring can be observed for the donor molecules, as the distance between sulfur atoms and the mean plane increases from 0.01 and 0.04 Å in SNTCNQ–DPTTA, to 0.04 and 0.09 Å in F2TCNQ–DPTTA and 0.06 and 0.09 Å in F4TCNQ–DPTTA. A reasonable interruption is that the degree of electron transfer from the donor molecules increases with the stronger acceptor, which makes the aromaticity of this 22 π-electron annulene decrease and leads to the more significant conformation distortion. Another method for the estimation of the CT characteristics was proposed by Kistenmacher et al for TCNQ, based on the band length ratio $r = c/(b + d)$ (c, b, d are bond lengths, see the note of Table S2 for the bond labelling, ESI†).[38] Table S2 in the ESI† summarizes the ratios of the neutral acceptor, fully ionized acceptor and charge-transfer complexes. The calculated ratio in SNTCNQ–DPTTA is very

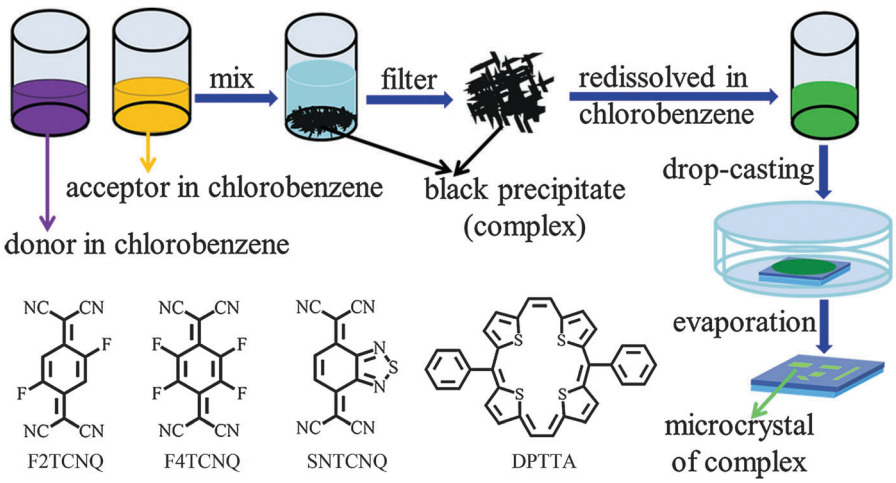

Scheme 1 Schematic illustration of the preparation of the self-assembled microcrystal for device fabrication and the chemical structure of compounds in this text.

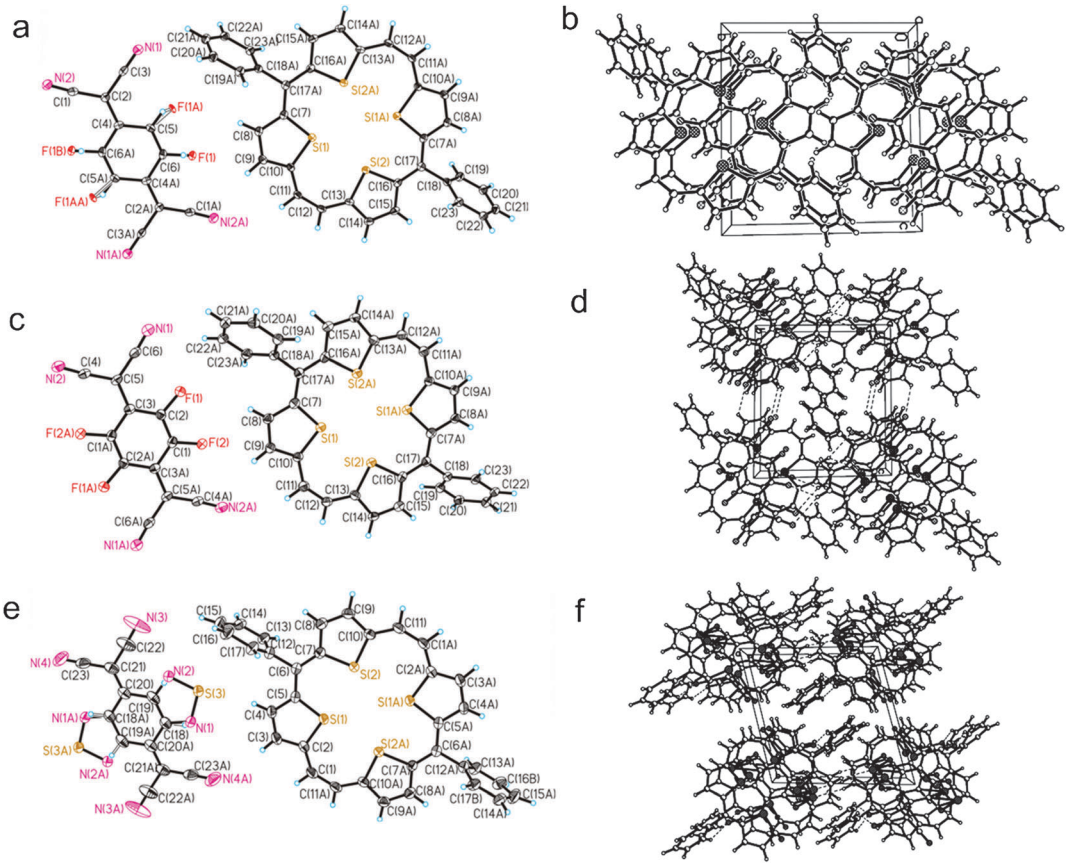

Fig. 1 Crystal structures of complexes. Molecular structure of F2TCNQ–DPTTA (a), F4TCNQ–DPTTA (c) and SNTCNQ–DPTTA (e). Stacking patterns of F2TCNQ–DPTTA (b), F4TCNQ–DPTTA (d) and SNTCNQ–DPTTA (f) (view along the *a*-axis, the dashed lines indicate the intermolecular hydrogen bonds). CCDC 1437142–1437144.

close to the value in neutral SNTCNQ, indicating that the CT is very weak. A large ratio, of up to 0.485, is calculated in F2TCNQ–DPTTA. Even a fully ionized F4TCNQ is revealed in F4TCNQ–DPTTA. The result suggests that the sequence of the degree of the CT interaction in these complexes is F4TCNQ–DPTTA > F2TCNQ–DPTTA ≫ SNTCNQ–DPTTA. This is consistent with the strength of electron accepting ability of the acceptors (Table S3 in the ESI†).

Fig. 1b, d and f illustrate the mixed packing mode of the molecules in the crystals, where donor and acceptor molecules alternate with nearly parallel orientation into columns along the *a*-axis. The dihedral angles between the mean plane of the donor and the acceptor are 1.18°, 1.19° and 1.75°, respectively. The overlap patterns between donor–acceptor molecules along the stacking direction are almost identical in these complexes (Fig. S3, ESI†). The acceptor molecule stacks over the center of the DPTTA core for ensuring the maximizing of intermolecular π–π interactions. This pattern is obviously different from what observed in the DPTTA–TCNQ complex, where the TCNQ molecule stacked over one half of the annulene ring. As the intermolecular electronic couplings are directly related to the intermolecular distance and overlapping patterns, this difference is expected to result in the variation of transport behaviour compared with the formerly reported TCNQ complex.

The intermolecular distance between the donor and the acceptor along the mixed-stack direction can be determined as half of the inter-plane distance of adjacent annulene rings, which are 3.41, 3.44 and 3.47 Å for F2TCNQ–DPTTA, F4TCNQ–DPTTA and SNTCNQ–DPTTA, respectively. Although the spacing is slightly larger than the sum of the van der Waals radii of the carbon atom (3.4 Å), it is still in the range of the characteristic distance for π–π stacking (3.3–3.6 Å for a small molecule semiconductor).[39] It shows a rough tendency that the donor–acceptor intermolecular distance decreases with the energy offset between the HOMO of the donor and the LUMO of the acceptor. As the donors distort from coplanar conformation more heavily in F4TCNQ–DPTTA, the size of the donor molecule increases along the perpendicular direction and results in the increase of the interplanar distance compared to F2TCNQ–DPTTA complexes. This will display a critical impact on the electronic coupling between the frontier orbits of donor and acceptor molecules along the stacking direction and determine the transport properties of these complexes, which will be discussed in detail in the quantum simulation section. Moreover, lateral intermolecular π–π interactions exist between neighbouring donor molecules in different columns (as shown in Fig. S3, ESI†), as the shortest carbon–carbon distance around 3.08 to 3.32 Å between thiophene units from two adjacent annulene

rings can be observed which is shorter than twice the van der Waals radius of carbon (3.40 Å). So, continuous direct π–π interactions among donor molecules are expected to serve as the charge transport path for holes. Besides these intermolecular π–π interactions, intermolecular hydrogen bonds, such as C15–H15···N1, C9–H9···N2A, C9–H9···F2 in F4TCNQ–DPTTA and C4–H4···S3, C16–H16···S3, C13–H13···N4, C16–H16···N2 in SNTCNQ–DPTTA, can be observed between donor and acceptor molecules in adjacent columns or along the stacking direction as shown in Fig. 1d and f.

The structures of the microcrystals grown on the SiO_2/Si substrate were examined using X-ray diffraction (XRD) (Fig. 2). Sharp Bragg reflections up to second or third order are observed and can be well indexed according to the crystallographic data for the bulk crystals. For F2TCNQ–DPTTA microcrystals, the XRD patterns show intense peaks at 8.14, 16.35, and 24.54°, which are indexed as (001), (002), and (003), respectively. In the case of F4TCNQ–DPTTA, the strong peaks at 7.92 and 15.89° are indexed as (001) and (002). For SNTCNQ–DPTTA, the strong peaks at 8.19 and 16.39° are indexed as (001) and (002). These diffraction patterns show that all those microcrystals grow with the *ab* plane parallel to the substrate.

In order to further verify the preferential growth direction of the micro-crystals, their selected-area electron diffraction (SAED) patterns were recorded in transmission electron microscopy characterization (Fig. 2). The highly symmetric diffraction patterns show the single crystalline nature of these microcrystals. The in-plane lattice distances were calculated as 0.777, 0.775 and 0.751 nm from the diffractive points for F2TCNQ–DPTTA, F4TCNQ–DPTTA, SNTCNQ–DPTTA samples, respectively. The distance coincides with the interplanar distance of the (100) plane of the corresponding bulk crystals. Correlation of TEM images and the corresponding diffraction patterns makes it clear that the microcrystals are all preferentially grown along the [100] direction (*a*-axis).

Transport properties

Charge transport properties were analyzed based on single crystal FETs with bottom-gate top-contact device configuration. Devices were directly prepared based on microcrystals of the complexes grown on SiO_2/Si substrates. A more detailed description of the fabrication process is available in the ESI.† All electrical measurements together with the device preparation were performed under an ambient atmosphere. The ideal transfer curves obtained from an individual single crystal device display unique V-shape characteristics, which demonstrate typical ambipolar behaviours (Fig. 3b, d and f). The negative gate voltage side of the V characteristics indicates the hole transport (V_D = −50 V), while the positive gate voltage side is dominated by the electron transport (V_D = 50 V).

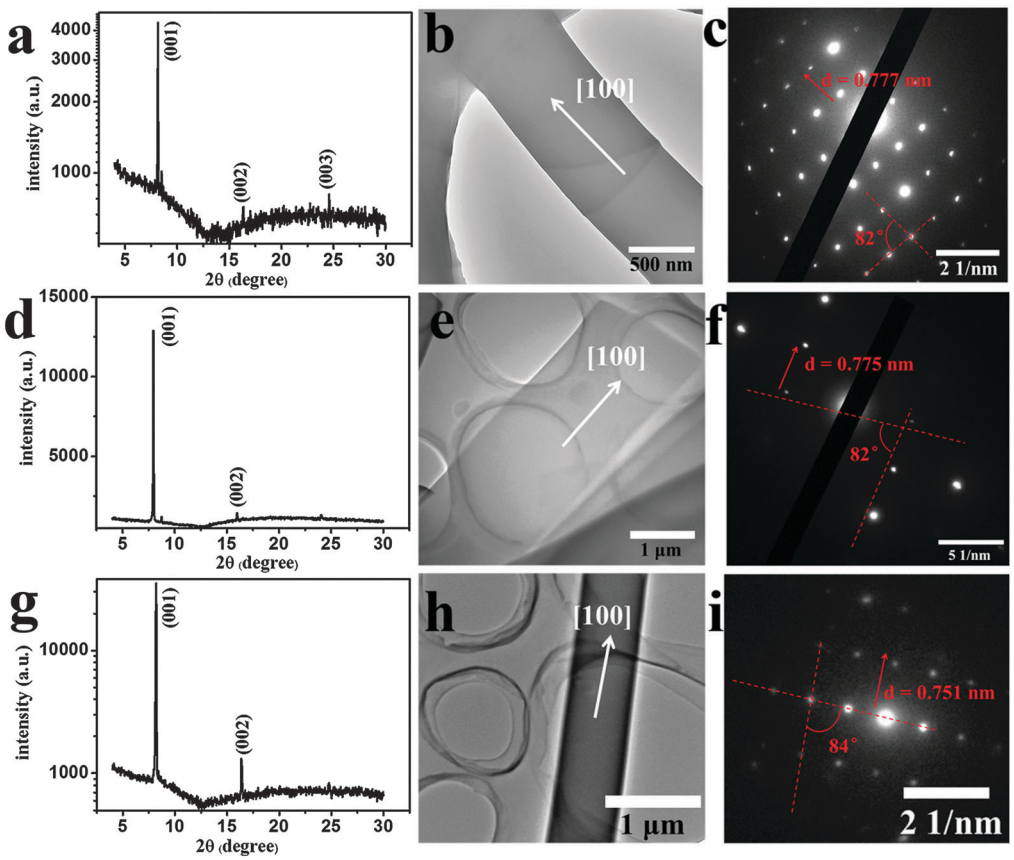

Fig. 2 X-ray diffraction, TEM images and the corresponding diffraction patterns of DPTTA-based microcrystals: (a–c) for F2TCNQ–DPTTA; (d–f) for F4TCNQ–DPTTA; (g–i) for SNTCNQ–DPTTA.

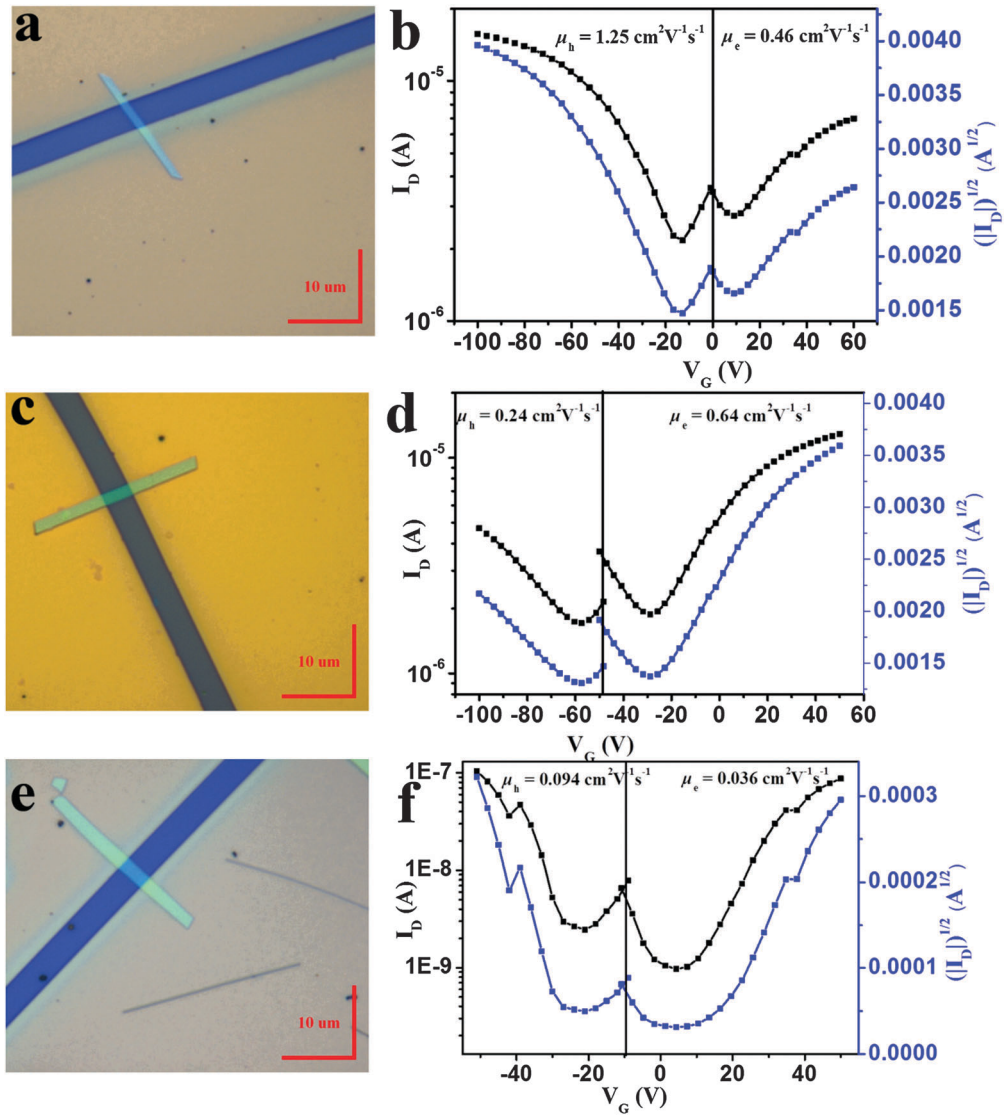

Fig. 3 Typical optical microscope view of a single-crystal device and the corresponding transfer characteristics: (a and b) for F2TCNQ–DPTTA, the ratio of channel width (W) and channel length (L), namely W/L = 0.30; (c and d) for F4TCNQ–DPTTA, W/L = 0.46; (e and f) for SNTCNQ–DPTTA, W/L = 0.58.

The highest hole and electron field-effect mobilities (μ) were calculated to be 1.57 cm^2 V^{-1} s^{-1} (μ_h) and 0.47 cm^2 V^{-1} s^{-1} (μ_e) for F2TCNQ–DPTTA. The hole mobility ranged from 0.73–1.57 cm^2 V^{-1} s^{-1} and the electron mobility ranged from 0.13–0.47 cm^2 V^{-1} s^{-1}. In contrast, for F4TCNQ–DPTTA single-crystal devices, the hole mobility ranged from 0.13–0.81 cm^2 V^{-1} s^{-1} and the electron mobility ranged from 0.43–1.18 cm^2 V^{-1} s^{-1}. Whereas for SNTCNQ–DPTTA single-crystal devices, poor hole mobility ranged from 0.02–0.1 cm^2 V^{-1} s^{-1} and the electron mobility ranged from 0.004–0.056 cm^2 V^{-1} s^{-1} were obtained. The corresponding output characteristics of transistors based on F2TCNQ–DPTTA, F4TCNQ–DPTTA and SNTCNQ–DPTTA single-crystals are presented in Fig. S4 in the ESI.† The regular output characteristic reveals good ohmic contact between the metal electrode and the semiconductor. The on/off current ratios (I_{on}/I_{off}) are all less than 10^2 orders of magnitude, even lower than 10 for F2TCNQ–DPTTA and F4TCNQ–DPTTA devices (Fig. S5 in the ESI†). The mobility distribution for these DPTTA-based field-effect devices is shown in Fig. S6 in the ESI.† Moreover, the device exhibits good stability in air even after months of storage in air. A typical evolution of performance *versus* storage time is also shown in Fig. S6 in the ESI.†

Theoretical calculations

Quantum simulations can be used to further investigate the donor–acceptor interaction, especially the electronic coupling along the mixed-stack direction caused by the super-exchange interaction. It is important for understanding the relationship between structure–transport properties of these D–A complexes. Here, the band structures as well as the intermolecular electronic coupling are calculated and presented. Geometry optimizations of the crystal structures were performed using the Perdew–Burke–Ernzerhof (PBE) exchange correlation functional,[40,41] and projector-augmented wave (PAW) basis sets as implemented

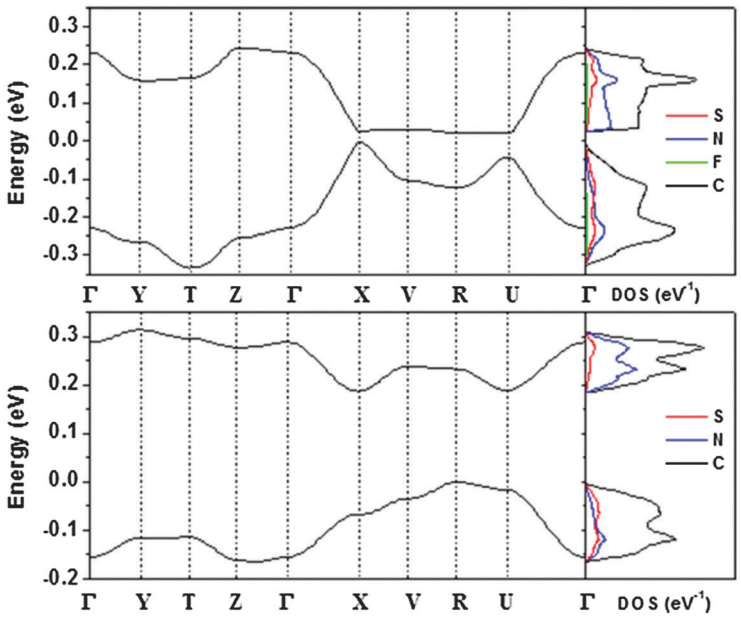

Fig. 4 Band structures of the 2,5-F2TCNQ–DPTTA crystal (top panel) and the 1-SNTCNQ–DPTTA crystal (bottom panel). The reciprocal coordinates of high-symmetry points are Γ = (0, 0, 0), Y = (0, 0.5, 0), T = (0, 0.5, 0.5), Z = (0, 0, 0.5), X = (0.5, 0, 0), V = (0.5, 0.5, 0), R = (0.5, 0.5, 0.5), U = (0.5, 0, 0.5).

in the Vienna *ab initio* simulation package (VASP).[42,43] However, the crystal structure data suggest that the fluorine atom appeared in 2,3,5,6-positions of the quinoid ring with 50% occupancy in F2TCNQ–DPTTA. The thiadiazolo-unit also disordered with a site-occupancy factor of 0.5 in SNTCNQ–DPTTA, possible structural models (labeled as 2,5-F2TCNQ–DPTTA; 3,6-F2TCNQ–DPTTA, 1-SNTCNQ–DPTTA and 2-SNTCNQ–DPTTA) are calculated respectively. The electronic band structures and density of states (DOS) were illustrated for 2,5-F2TCNQ–DPTTA and 1-SNTCNQ–DPTTA in Fig. 4, with other systems and disorder cases illustrated in Fig. S7 (ESI†).

For F2TCNQ–DPTTA and F4TCNQ–DPTTA, both the valence band (VB) and conduction band (CB) widths are relatively large, in the range of 316–329 and 224–239 meV. In contrast, for SNTCNQ–DPTTA, both the VB and CB widths are relatively small (165 and 127 meV, respectively). For all systems, the largest dispersion occurs along the alternate stacking direction and displays quasi mirror symmetry for the VBs and CBs (see Γ–X in Fig. 4). Since along the alternate stacking direction, the nearest-neighboured D or A molecules are too far away to interact directly with each other, a super-exchange mechanism is suggested.[30] In order to understand the origin of large dispersion of the band structure, a detailed analysis of super-exchange coupling is needed.

Although intermolecular direct coupling has been widely investigated,[44] there are few reports on bridge mediated super-exchange coupling in organic semiconductors. Based on a localized charge model, charge transport is not allowed along the D–A mixed-stack direction, since the nearest-neighbored D (or A) molecules are too far away to interact directly with each other. In fact, for hole (electron) transport, an effective electronic coupling between adjacent D (A) molecules is manifested by a super-exchange mechanism, where the in-between A (D) molecule is taken as the bridge, as illustrated in Scheme S2 (ESI†). The super-exchange coupling can be written approximately as follows:[32]

$$t_{12}^{\mathrm{eff}} \approx \sum_{\mathrm{b}\in\mathrm{B}} \frac{\tilde{V}_{1\mathrm{b}}\tilde{V}_{\mathrm{b}2}}{E-\tilde{\varepsilon}_{\mathrm{b}}} \quad (1)$$

The super-exchange interaction depends quadratically on intermolecular coupling between the bridge moiety and the adjacent molecule 1 and molecule 2, labelled as $\tilde{V}_{1\mathrm{b}}$, $\tilde{V}_{\mathrm{b}2}$, these two parameters reflect the intermolecular interaction, which correlates with the intermolecular stacking distance and the packing pattern between donor and acceptor moieties. On the other hand, the super-exchange coupling is inversely proportional to the energy difference (ΔE) between E (the adiabatic energy) and $\tilde{\varepsilon}_{\mathrm{b}}$ (bridge energy). Here, ΔE can be approximately regarded as energy difference between IP (ionized potential) of the isolated donor and EA (electron affinity) of the isolated acceptor. Therefore, tuning the intermolecular coupling or energy level alignment will be an effective way to design high charge transport materials. Considering the coupling of the HOMO of the donor and the LUMO of the acceptor makes a dominant contribution in this case, $\tilde{V}_{1\mathrm{b}}$ equal to $\tilde{V}_{\mathrm{b}2}$, the above formula can be simplified further:

$$t_{12}^{\mathrm{eff}} \approx \frac{V_{\mathrm{H_D-L_A}}{}^2}{\Delta E} \quad (2)$$

With the increase of the π–π stacking distance from 3.41 to 3.47 Angstrom from F2TCNQ to SNTCNQ, intermolecular electronic coupling decreases from 295 meV to 217 meV. However, with the increase of redox potentials (EA) from SNTCNQ, F2TCNQ to F4TCNQ, the energy difference (ΔE) with DPTTA decreases accordingly. Therefore, SNTCNQ–DPTTA reveals the smallest super-exchange coupling. F2TCNQ–DPTTA and F4TCNQ–DPTTA

Table 1 Electronic coupling ($V_{H_D-L_A}^2$) between the HOMO of a donor and the LUMO of an acceptor; energy difference (ΔE) between IPD and EAA, where IPD and EAA represent the vertical ionization potential of DPTTA and affinity energy of acceptor molecules, respectively; the amount of charge transfer (δe) between donor and acceptor molecules. Calculated at the B3LYP/6-31g(d) level. Energy in meV

				Energy-splitting		Partition-based	
Crystal	$V_{H_D-L_A}^2$	ΔE	δe	t_{hole}	t_{elec}	t_{hole}	t_{elec}
2,5-F2TCNQ–DPTTA	295	2150	0.441	80.3	89.0	85.1	86.2
F4TCNQ–DPTTA	287	1910	0.531	84.4	95.4	90.0	91.2
1-SNTCNQ–DPTTA	217	2395	0.280	61.1	65.6	37.1	36.7

display similar magnitude super-exchange coupling. Due to the environmental polarization effect, the energy splitting method overestimates super-exchange coupling significantly for the SNTCNQ–DPTTA system. It has been found that with the increase of charge transfer, the super-exchange coupling increases accordingly. The disorder of fluorine and thiadiazolo units has little effect on electronic coupling in these cases (Table 1).

Fig. 5 shows the main charge transport pathway through super-exchange coupling (t^{eff}) in the mixed stacking (…–D–A–D–A–…) direction, and direct coupling (t^{direct}) in the separated stacking (…–A–A–A–… and …–D–D–D–…) direction. For F2TCNQ–DPTTA and F4TCNQ–DPTTA, the electronic coupling is large for both holes and electrons along the mixed stacking direction in the range of 85–91 meV. For SNTCNQ, the electronic coupling is 37 meV for holes and electrons, nearly one half of the other systems, consistent with above intermolecular packing and energy alignment analysis. And thus, although relative charge transport properties have a large difference, ambipolar charge transport can be obtained for all of the three systems.

It is worthy of note that super-exchange coupling could be tuned with the donor–acceptor energy alignment and the donor–acceptor interaction, but this effect is not so significant in the calculated results for a complex with F2TCNQ and F4TCNQ acceptors, as the donor–acceptor inter-plane distance in F2TCNQ–DPTTA and F4TCNQ–DPTTA increases with the charge transfer ratio. In fact, charge transport in a realistic device is a complex question, which depends on the electric field, charge injection, dielectric materials, interface effect, grain boundary, defect, charge carrier density and so on. Comparing F4TCNQ–DPTTA with F2TCNQ–DPTTA and SNTCNQ–DPTTA, F4TCNQ–DPTTA has the lowest LUMO energy level and then the lower HOMO energy level as well, which may be benefit to the electron injection and harmful to hole injection. F2TCNQ–DPTTA and SNTCNQ–DPTTA reveal higher HOMO and LUMO energy than that of F4TCNQ–DPTTA, which is benefit to hole transport but harmful to electron transport. Therefore, it may be a possible reason that the electron mobility is higher than that of the hole mobility in the F4TCNQ system. The hole mobility is higher than the electron mobility in F2TCNQ and SNTCNQ systems. Meanwhile, a stronger donor–acceptor interaction will result in the more rapid formation of the complexes, which may lead to a relatively low quality of the crystals obtained. The existence of defects and traps will deteriorate the charge transport properties, and lead to mismatching between the experimental and theoretical results.

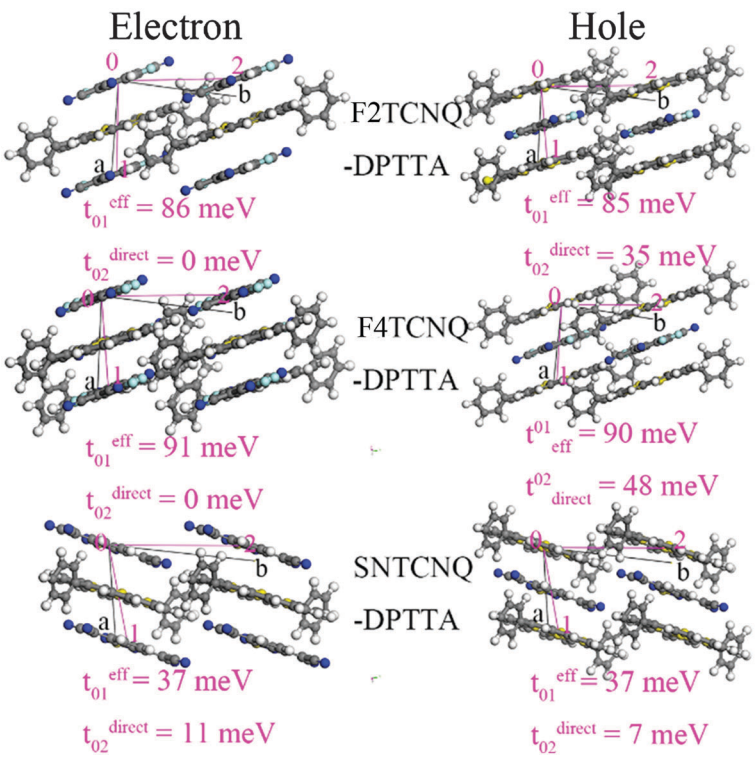

Fig. 5 Illustration of the most important charge-transport pathways for holes and electrons. Calculated at the DFT-B3LYP/6-31g(d) level.

Conclusions

In conclusion, we have successfully prepared three new sulfur-bridged annulene-based donor–acceptor charge-transfer complexes and investigated their transport properties using an organic single crystal field-effect transistor device. The difference in the electron affinity of acceptors allows us to tune and optimize the transport properties by taking advantage of the donor–acceptor interaction *via* charge transfer. The superior ambipolar charge injection and transport with a remarkably high mobility, up to 1.57 $cm^2 V^{-1} s^{-1}$ for holes and 0.47 $cm^2 V^{-1} s^{-1}$ for electrons, was demonstrated. Various short contacts and the direct π–π interaction in the complexes, resulting in a densely two-dimensional or three-dimensional interaction network, provide excellent conduction paths, which are critical for efficient carrier transport.

Through electronic band structure and super-exchange coupling calculations, we rationalized the origin of the excellent ambipolar properties. The donor–acceptor interactions and their energy alignment will influence the charge transport properties significantly. The super-exchange transport mechanism and the structure–property relationship investigated in this research will provide an important guideline for the future design of this class organic semiconductor.

With these fundamental understandings, we anticipate that the combination of hole-conducting (donor) and electron-conducting (acceptor) molecules into single-crystal complexes could be viewed as a successful strategy towards high-mobility ambipolar field effect transistors. Through the combination of the experimental and theoretical study, the concluded correlation between the charge transport, packing mode and donor–acceptor interaction from this research will pave an important pathway, as well as provide a guideline for the future design of this class organic semiconductor. Furthermore, we are convinced that unprecedented opportunities will come and more success is expectable in this field.

Acknowledgements

The authors acknowledge the financial support from National Natural Science Foundation of China (21290191, 21372227, 21303213) and the Strategic Priority Research Program of the Chinese Academy of Sciences (Grant No. XDB12000000).

Notes and references

1 C. Wang, H. Dong, W. Hu, Y. Liu and D. Zhu, *Chem. Rev.*, 2012, **112**, 2208–2267.
2 J. Lee, A. R. Han, H. Yu, T. J. Shin, C. Yang and J. H. Oh, *J. Am. Chem. Soc.*, 2013, **135**, 9540–9547.
3 H. N. Tsao, D. M. Cho, I. Park, M. R. Hansen, A. Mavrinskiy, Y. Yoon do, R. Graf, W. Pisula, H. W. Spiess and K. Mullen, *J. Am. Chem. Soc.*, 2011, **133**, 2605–2612.
4 B. Sun, W. Hong, Z. Yan, H. Aziz and Y. Li, *Adv. Mater.*, 2014, **26**, 2636–2642.
5 Y. Yuan, G. Giri, A. L. Ayzner, A. P. Zoombelt, S. C. Mannsfeld, J. Chen, D. Nordlund, M. F. Toney, J. Huang and Z. Bao, *Nat. Commun.*, 2014, **5**, 3005–3013.
6 J. Li, X. Qiao, Y. Xiong, H. Li and D. Zhu, *Chem. Mater.*, 2014, **26**, 5782–5788.
7 H. Hwang, D. Khim, J.-M. Yun, E. Jung, S.-Y. Jang, Y. H. Jang, Y.-Y. Noh and D.-Y. Kim, *Adv. Funct. Mater.*, 2015, **25**, 1146–1156.
8 S. Z. Bisri, C. Piliego, J. Gao and M. A. Loi, *Adv. Mater.*, 2014, **26**, 1176–1199.
9 T. D. Anthopoulos, S. Setayesh, E. Smits, M. Cölle, E. Cantatore, B. de Boer, P. W. M. Blom and D. M. de Leeuw, *Adv. Mater.*, 2006, **18**, 1900–1904.
10 M. Irimia-Vladu, E. D. Glowacki, P. A. Troshin, G. Schwabegger, L. Leonat, D. K. Susarova, O. Krystal, M. Ullah, Y. Kanbur, M. A. Bodea, V. F. Razumov, H. Sitter, S. Bauer and N. S. Sariciftci, *Adv. Mater.*, 2012, **24**, 375–380.
11 H.-S. Seo, D.-K. Kim, J.-D. Oh, E.-S. Shin and J.-H. Choi, *J. Phys. Chem. C*, 2013, **117**, 4764–4770.
12 M. Melucci, L. Favaretto, M. Zambianchi, M. Durso, M. Gazzano, A. Zanelli, M. Monari, M. G. Lobello, F. De Angelis, V. Biondo, G. Generali, S. Troisi, W. Koopman, S. Toffanin, R. Capelli and M. Muccini, *Chem. Mater.*, 2013, **25**, 668–676.
13 T. Hasegawa, K. Mattenberger, J. Takeya and B. Batlogg, *Phys. Rev. B: Condens. Matter Mater. Phys.*, 2004, **69**, 245115.
14 S. Horiuchi, T. Hasegawa and Y. Tokura, *J. Phys. Soc. Jpn.*, 2006, **75**, 051016.
15 K. V. Rao and S. J. George, *Chem. – Eur. J.*, 2012, **18**, 14286–14291.
16 K. R. Leight, B. E. Esarey, A. E. Murray and J. J. Reczek, *Chem. Mater.*, 2012, **24**, 3318–3328.
17 Y. L. Lei, Y. Jin, D. Y. Zhou, W. Gu, X. B. Shi, L. S. Liao and S. T. Lee, *Adv. Mater.*, 2012, **24**, 5345–5351.
18 W. Yu, X. Y. Wang, J. Li, Z. T. Li, Y. K. Yan, W. Wang and J. Pei, *Chem. Commun.*, 2013, **49**, 54–56.
19 Y. Li, W. Wang, W. R. Leow, B. Zhu, F. Meng, L. Zheng, J. Zhu and X. Chen, *Small*, 2014, **10**, 2776–2781.
20 H.-D. Wu, F.-X. Wang, Y. Xiao and G.-B. Pan, *J. Mater. Chem. C*, 2013, **1**, 2286–2289.
21 T. Wakahara, P. D'Angelo, K. Miyazawa, Y. Nemoto, O. Ito, N. Tanigaki, D. D. C. Bradley and T. D. Anthopoulos, *J. Am. Chem. Soc.*, 2012, **134**, 7204–7206.
22 H. T. Black and D. F. Perepichka, *Angew. Chem., Int. Ed.*, 2014, **53**, 2138–2142.
23 J. y. Tsutsumi, S. Matsuoka, S. Inoue, H. Minemawari, T. Yamada and T. Hasegawa, *J. Mater. Chem. C*, 2015, **3**, 1976–1981.
24 S. K. Park, S. Varghese, J. H. Kim, S. J. Yoon, O. K. Kwon, B. K. An, J. Gierschner and S. Y. Park, *J. Am. Chem. Soc.*, 2013, **135**, 4757–4764.
25 J. Zhang, H. Geng, T. S. Virk, Y. Zhao, J. Tan, C. A. Di, W. Xu, K. Singh, W. Hu, Z. Shuai, Y. Liu and D. Zhu, *Adv. Mater.*, 2012, **24**, 2603–2607.
26 J. Zhang, J. Tan, Z. Ma, W. Xu, G. Zhao, H. Geng, C. Di, W. Hu, Z. Shuai, K. Singh and D. Zhu, *J. Am. Chem. Soc.*, 2013, **135**, 558–561.

27 Y. Qin, J. Zhang, X. Zheng, H. Geng, G. Zhao, W. Xu, W. Hu, Z. Shuai and D. Zhu, *Adv. Mater.*, 2014, **26**, 4093–4099.
28 K. P. Goetz, D. Vermeulen, M. E. Payne, C. Kloc, L. E. McNeil and O. D. Jurchescu, *J. Mater. Chem. C*, 2014, **2**, 3065–3076.
29 A. K. Blackburn, A. C. Sue, A. K. Shveyd, D. Cao, A. Tayi, A. Narayanan, B. S. Rolczynski, J. M. Szarko, O. A. Bozdemir, R. Wakabayashi, J. A. Lehrman, B. Kahr, L. X. Chen, M. S. Nassar, S. I. Stupp and J. F. Stoddart, *J. Am. Chem. Soc.*, 2014, **136**, 17224–17235.
30 L. Zhu, Y. Yi, Y. Li, E. G. Kim, V. Coropceanu and J.-L. Bredas, *J. Am. Chem. Soc.*, 2012, **134**, 2340–2347.
31 L. Zhu, Y. Yi, A. Fonari, N. S. Corbin, V. Coropceanu and J.-L. Brédas, *J. Phys. Chem. C*, 2014, **118**, 14150–14156.
32 H. Geng, X. Zheng, Z. Shuai, L. Zhu and Y. Yi, *Adv. Mater.*, 2015, **27**, 1443–1449.
33 D. Vermeulen, L. Y. Zhu, K. P. Goetz, P. Hu, H. Jiang, C. S. Day, O. D. Jurchescu, V. Coropceanu, C. Kloc and L. E. McNeil, *J. Phys. Chem. C*, 2014, **118**, 24688–24696.
34 D. Jérome, *Chem. Rev.*, 2004, **104**, 5565–5591.
35 T. J. Emge, *J. Chem. Phys.*, 1982, **77**, 3188–3197.
36 J. S. Chappell, A. N. Bloch, W. A. Bryden, M. Maxfield, T. O. Poehler and D. O. Cowan, *J. Am. Chem. Soc.*, 1981, **103**, 2442–2443.
37 X. Chi, C. Besnard, V. K. Thorsmølle, V. Y. Butko, A. J. Taylor, T. Siegrist and A. P. Ramirez, *Chem. Mater.*, 2004, **16**, 5751–5755.
38 T. J. Kistenmacher, T. J. Emge, A. N. Bloch and D. O. Cowan, *Acta Crystallogr., Sect. B: Struct. Crystallogr. Cryst. Chem.*, 1982, **38**, 1193–1199.
39 Y. Zhao, Y. Guo and Y. Liu, *Adv. Mater.*, 2013, **25**, 5372–5391.
40 J. P. Perdew, K. Burke and M. Ernzerhof, *Phys. Rev. Lett.*, 1996, **77**, 3865–3868.
41 J. P. Perdew, K. Burke and M. Ernzerhof, *Phys. Rev. Lett.*, 1997, **78**, 1396.
42 G. Kresse and J. Furthmüller, *Phys. Rev. B: Condens. Matter Mater. Phys.*, 1996, **54**, 11169–11186.
43 G. Kresse and J. Furthmüller, *Comput. Mater. Sci.*, 1996, **6**, 15–50.
44 Z. Shuai, H. Geng, W. Xu, Y. Liao and J. M. Andre, *Chem. Soc. Rev.*, 2014, **43**, 2662–2679.